WALAILAK JOURNAL
http://wjst.wu.ac.th Engineering and Physical Sciences

Numerical Based Heat Transfer and Friction Factor Correlations of Rectangular Ducts Roughened With Transverse Perforated Baffles

Sunil CHAMOLI* and Narender Singh THAKUR

Centre for Energy and Environment, National Institute of Technology, Hamirpur 177005, India

(*Corresponding author's e-mail: mech.chamoli@gmail.com)

Received: 13 December 2012, Revised: 10 February 2013, Accepted: 23 August 2013

Abstract

A numerical investigation has been carried out for a range of flow and geometrical parameters in order to analyze the effect of transverse perforated baffles attached on the heated wall of rectangular duct on heat transfer and friction factor. An increase in heat transfer and friction loss over a smooth surface has been observed for duct having perforated baffles as a roughness element. Numerical results have been used to develop the Nusselt number and friction factor correlations as a function of flow and geometrical parameters for predicting performance of the system having investigated the type of roughness elements.

Keywords: CFD, Nusselt number, perforated baffles, open area ratio

Introduction

Heat transfer enhancement in a single phase at a low and moderate Reynolds number has been a subject of intensive research over the years. It has numerous applications, such as the cooling of electronics systems, internal cooling inside turbine blades, compact heat exchangers, biomedical devices, solar air heaters etc. Many techniques based on both active and passive methods have been proposed to enhance heat transfer in these applications. Among these methods, one can find systems involving vortex generators, such as ribs, baffles and winglets. Disturbance promoters increase fluid mixing and interrupt the development of thermal boundary layers, leading to enhancement of heat transfer. The solid baffles increase the heat transfer, accompanied with a high increase in pressure drop. However, in the case of solid baffles, a large hot spot is generated just downstream from the baffle, leading to heat transfer deterioration around that position, as a result of flow separation in the form of a flow recirculation. To overcome this adverse effect, perforated baffles are used, as the perforated element allows part of the flow to pass through holes; thus the hot zone and form drag are reduced. The baffles enhance the heat transfer rate, but a considerable increase in pumping power is also reported, which makes the system ineffective by reducing the thermal performance. Designers and engineers are looking for some modification in the baffles to increase the heat transfer rate without much increase in friction factor. On changing the shape of ribs or baffles, a high increase in the heat transfer rate was reported, with less of an increase in pumping power; this was investigated experimentally and numerically [1-17]. Studies [18-26] of perforated baffles show that the perforated elements enhance the heat transfer rate with a lower pressure loss penalty.

Numerical analysis of laminar heat transfer in a channel with staggered diamond shaped baffles was carried out by [12] and found that the thermal performance of the 5° - 10° diamond baffle is found to be higher than that of the flat baffle. Promvonge *et al*. [15] explored the laminar flow and heat transfer characteristics in a square channel with 30° inline angled baffle turbulators and found the maximum thermal enhancement factors for the baffle with PR = 1, 1.5 and 2 were about 3.6, 3.8 and 4 at BR = 0.3, 0.2 and 0.15, respectively. Kwankaomeng and Promvonge [16] reported numerically the laminar heat transfer in a square duct with 30^o inclined baffles on one wall; the study revealed that the Nusselt number ratio and the maximum thermal enhancement factor values for using the angled baffle were, respectively, about 7.9 and 3.1 at Re = 2000, B.R = 0.3 and PR = 1.5. In an another study [17] reported numerically the periodic laminar flow and heat transfer in a channel with 45° staggered V baffles, and it was found that the optimum thermal enhancement factor is around 2.6 at a baffle height of 0.15 times of the channel height for v baffle pointing upstream, while is about 2.75 at a baffle height of 0.2 times for the V baffle pointing downstream.

Most of the investigation on turbulent flow in perforated ribs or baffles, cited above, has considered the heat transfer characteristics for spacing ratio and open area ratio only. In the present work, a numerical computation for 2 dimensional rectangular channel flows over a perforated baffles mounted on the heated channel wall was performed, with the main aim being to study the changes in the flow pattern and heat transfer performance, including the effect of baffle blockage in the case of perforated baffles. The CFD based results of heat transfer and pressure drop were used to develop correlation, which may be useful to designers.

Nomenclature

d	hole diameter (m)
D_h	hydraulic diameter of duct (m)
e	height of the baffle (m)
e/H	baffle height to duct height ratio
f	friction factor
H	height of the duct (m)
h	heat transfer coefficient (W/m^2 K)
L	length of test section (m)
l	hole position from base of baffle (m)
l/e	hole position to baffle height ratio
Nu	Nusselt number
P	spacing between baffles (m)
P/e	pitch to baffle height ratio
ΔP	pressure drop across test section (Pa)
Re	Reynolds number
T	temperature (K)
U	mean velocity (m/s)

Greek

ρ	density of air at bulk mean air temperature (kg/m^3)
β	open area ratio
μ	dynamic viscosity of air (Pa-s)

Subscript

s	smooth duct

Computational domain

Baffle geometry

The system of interest is a horizontal plane channel with perforated baffles along the upper channel wall, as shown in **Figure 1**. The channel dimension and range of parameters in the study was considered from [26] and is used for code validation of experimental and numerical results. The channel height is set to H = 38.4 mm while the channel length is 1,652 mm and the aspect ratio (W/H) is 7.77. The geometrical parameters of investigation are Reynolds number (Re) 2700 - 11150, Relative baffle height (e/H) 0.285 -

0.657, Relative roughness pitch (p/e) 7.21 - 28.84, Open area ratio (β) 12 - 44 % and the thickness of baffle, considered as (δ) 0.9 mm.

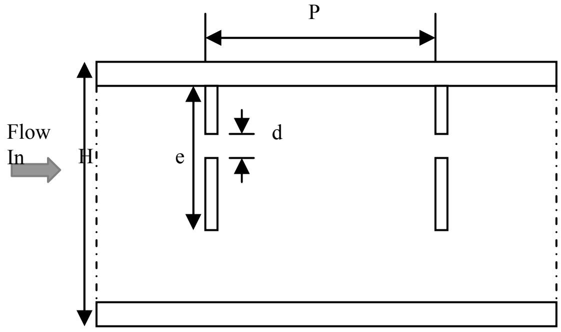

Figure 1 Channel geometry and sectional view of computational domain.

Boundary conditions

For a full length perforated baffle channel, a uniform air velocity is introduced at the inlet while a pressure outlet condition is applied at the exit. A constant velocity of air with 300 K (Pr = 0.707) is assumed in the flow direction. The physical properties of the air have been assumed to remain constant at a mean bulk temperature. Impermeable boundary and no-slip wall conditions have been implemented over the channel walls. The constant flux of 1,000 W/m^2 was given at the perforated baffled wall while the opposite side was kept at adiabatic wall condition. A constant 300 K temperature condition is employed for perforated baffles, the same as the initial air temperature.

Mathematical modeling

The phenomenon under consideration is governed by the steady 2-Dimensional form of continuity, the time averaged incompressible Navier-Stokes equations and the energy equation. In the Cartesian tensor system these equations can be written as;

Continuity:

$$\left(\frac{\partial U_j}{\partial x_j}\right) = 0 \tag{1}$$

Momentum:

$$\frac{DU_i}{Dt} = -\frac{1}{\rho}\frac{\partial p}{\partial x_i} + \frac{\partial}{\partial x_j}\left((\nu+\nu_t)\frac{\partial Uj}{\partial x_j}\right) \tag{2}$$

Energy:

$$\frac{DT}{Dt} = \frac{\partial}{\partial x_j}\left[\left(\frac{\nu}{\Pr} + \frac{\nu_t}{\sigma_t}\right)\frac{\partial T}{\partial x_j}\right] \tag{3}$$

The second order upwind scheme was used to discreitize the governing equations, to decouple it from the simple algorithm and to provide a solution using a finite volume approach [27]. The solution was considered converged when the normalized residual values were less than 10^{-8} for energy, while for other variables it was 10^{-5}.

The parameters of investigation in the study are the Reynolds number defined as;

$$\mathrm{Re} = \frac{\rho U D_h}{\mu}, \tag{4}$$

the friction factor is calculated as;

$$f = \frac{(\Delta p / L) D_h}{(1/2)\rho U^2}, \tag{5}$$

the heat transfer is measured by local Nusselt number defined as;

$$Nu_x = \frac{h_x D_h}{k}, \tag{6}$$

the average Nusselt number along the whole length is calculated as;

$$Nu = \frac{1}{L} \int Nu_x \partial x \tag{7}$$

and the thermal enhancement factor is defined as;

$$\eta = \frac{(Nu / Nu_s)}{(f / f_s)^{1/3}}. \tag{8}$$

Nu_s and f_s are the Nusselt number and the friction factor for smooth channel respectively.

A regular grid was used throughout the channel flow domain as shown in **Figure 2**. A grid independence test was performed in order to obtain the grid independent solution. It was found that the difference in the heat transfer coefficient between the results of the grid system of about 396080 and 528050 is less than 4 %, as shown in **Figure 3**. Considering both convergent time and solution precision, the grid system of 396080 was adopted for the computational model.

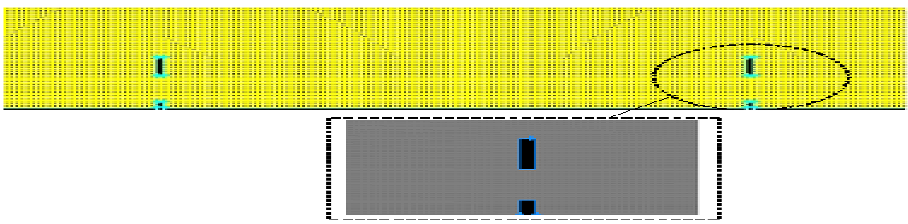

Figure 2 Grid arrangement for perforated baffled channel flow.

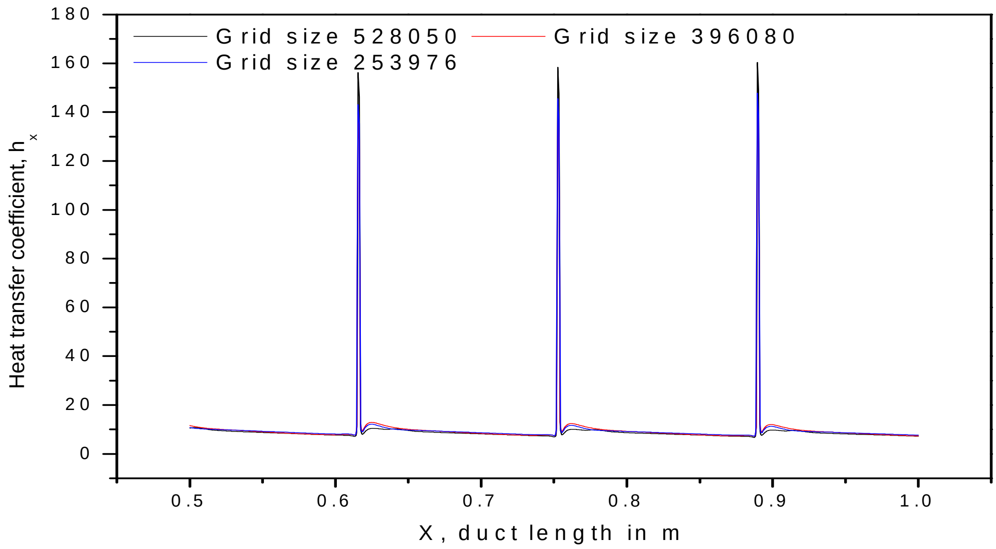

Figure 3 Effect of grid densities on heat transfer coefficient at Re = 2700, e/H = 0.495, p/e = 7.21, β = 24 %.

Results and discussion

Selection and validation of turbulence model

Different models, namely K-Ɛ (standard, RNG, realizable) and k-ω (standard and SST), have been tested for smooth channel to compare with the exact solutions. The results obtained by different models have been compared with the Dittus-Boelter empirical correlation for the Nusselt number given below for smooth channel.

$$NU_S = 0.023\,\mathrm{Re}^{0.8}\,\mathrm{Pr}^{0.4} \tag{9}$$

Figure 4 shows the variation of the Nusselt number with the Reynolds number for different models, and the results are compared with the empirical correlation of Dittus-Boelter. It is seen from graph that the k-Ɛ RNG turbulence model results are found to be in good agreement with the empirical results. The 4 % mean absolute deviation is found between the K-Ɛ RNG model and the empirical Dittus-Boelter correlation. Thus, for the present simulation, the K-Ɛ RNG model has been employed to simulate the flow and heat transfer.

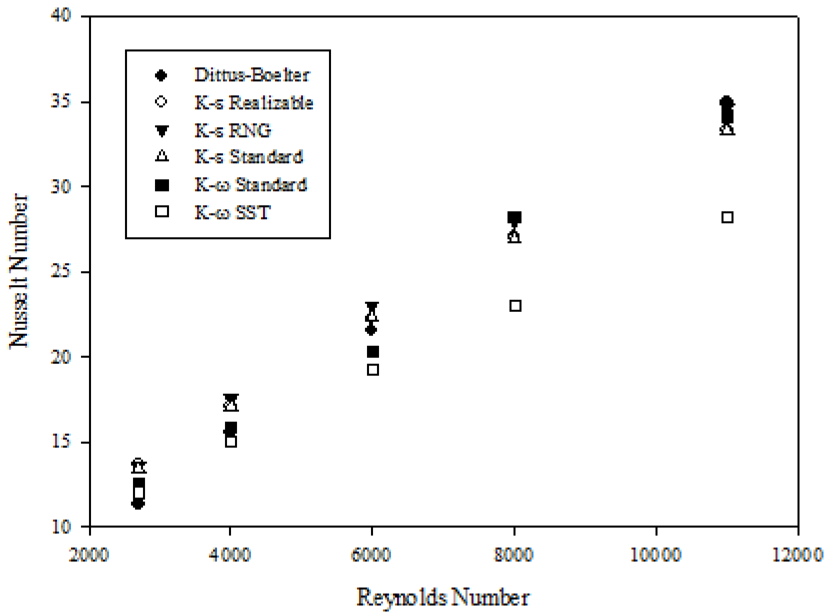

Figure 4 Comparison between Nusselt number predictions of different CFD models with Dittus- Boelter empirical correlation for smooth duct.

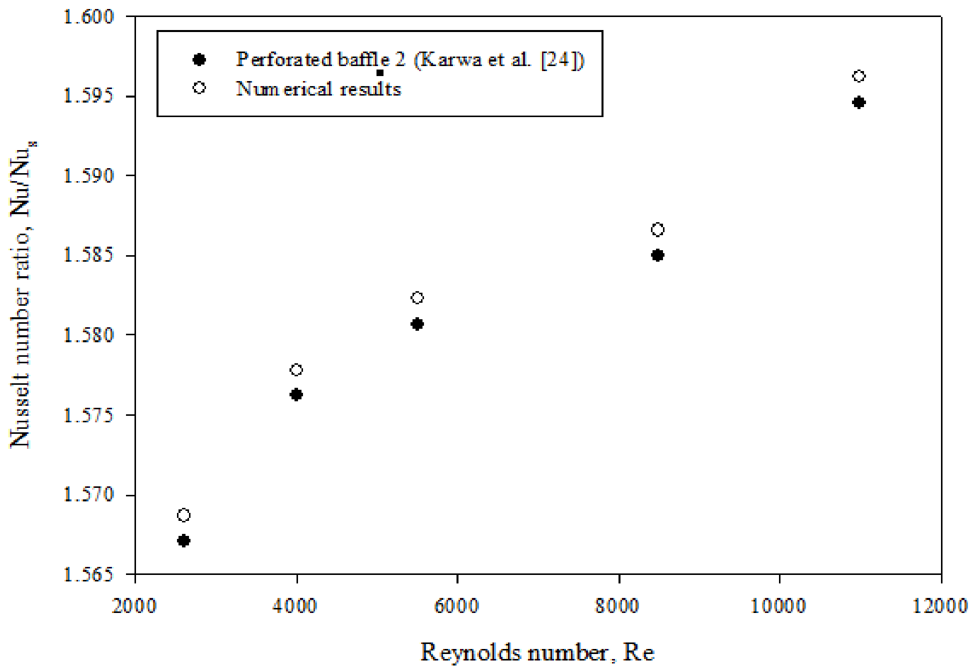

Figure 5 Comparison of experimental and numerical results.

Code validation

In **Figure 5** numerical results are compared with the experimental results of [24]. It is seen that the numerical results are found to be in good agreement with the experimental results. This ensures the accuracy of the numerical data obtained from the present work. Thus, different parameters, viz. relative pitch, open area ratio are considered for further analysis, in order to demonstrate completely the effect of perforation and flow reattachment on heat transfer and friction factor.

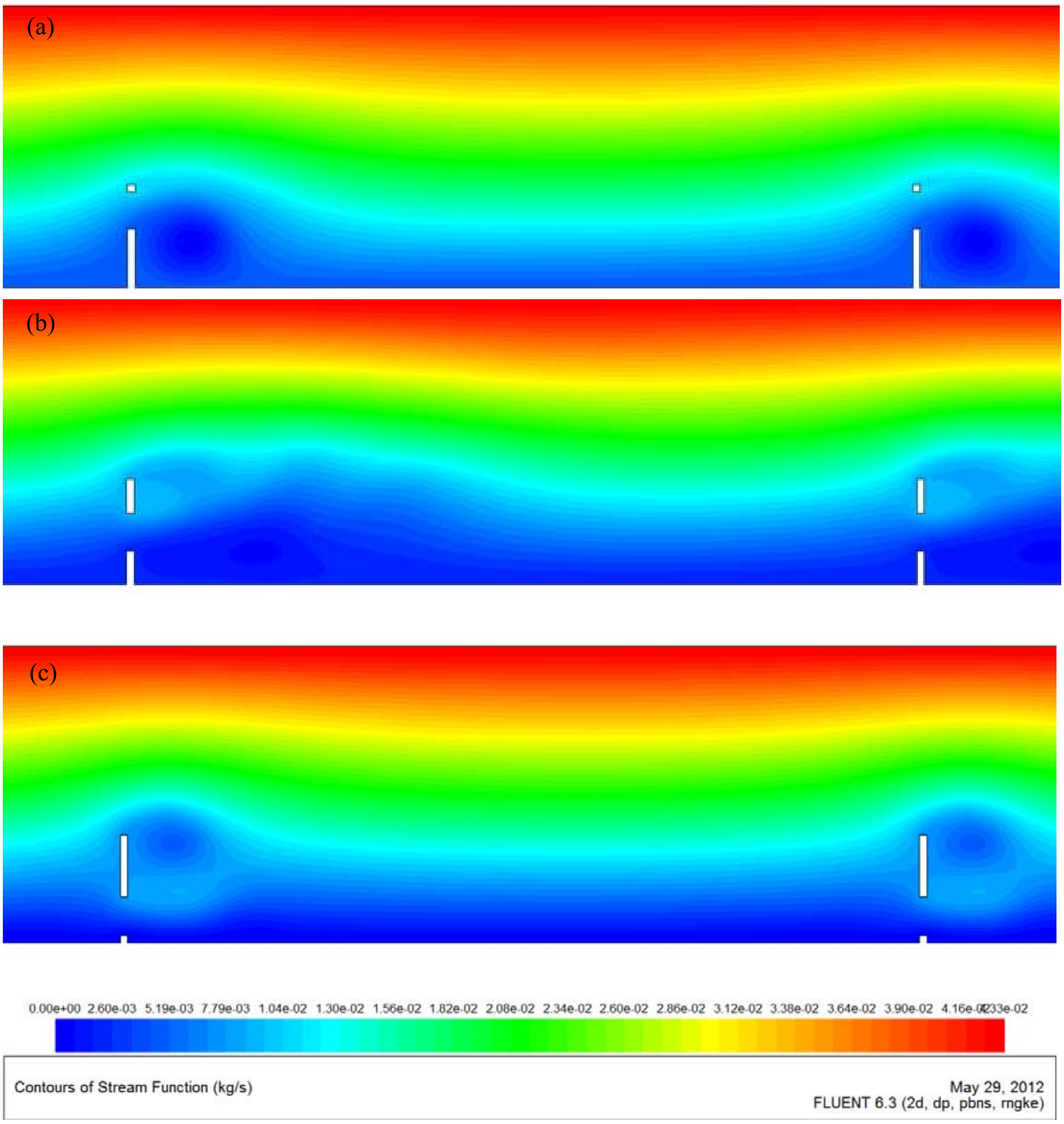

Figure 6 Contour plot of stream function of e/H = 0.4, P/e = 7.21, β = 12 %, Re = 2600: (a) l/e = 0.571 (b) l/e = 0.5 (c) l/e = 0.429.

Flow structure

The time averaged channel flow structure in the presence of perforated baffles can be easily discerned by considering the stream function plots in **Figure 6**. The Figure presents stream functions of turbulent channel flow through perforated baffles using the K-ε turbulence model for l/e = 0.571, 0.5, 0.429, respectively. Here, the streamlines in the perforated baffles are presented. It is shown that the largest recirculation zone can be found in the l/e = 0.571. The larger the position of hole from the heated surface, the longer the recirculation zone. The same phenomenon is observed for pathlines shown in **Figure 7**. **Figure 8** shows the effect of open area ratio, and it is seen from this figure that, on increasing the open area ratio, the fluid flow spent just downstream and jet impingement on the heated surface is not observed, and caused low rate of heat transfer from the surface.

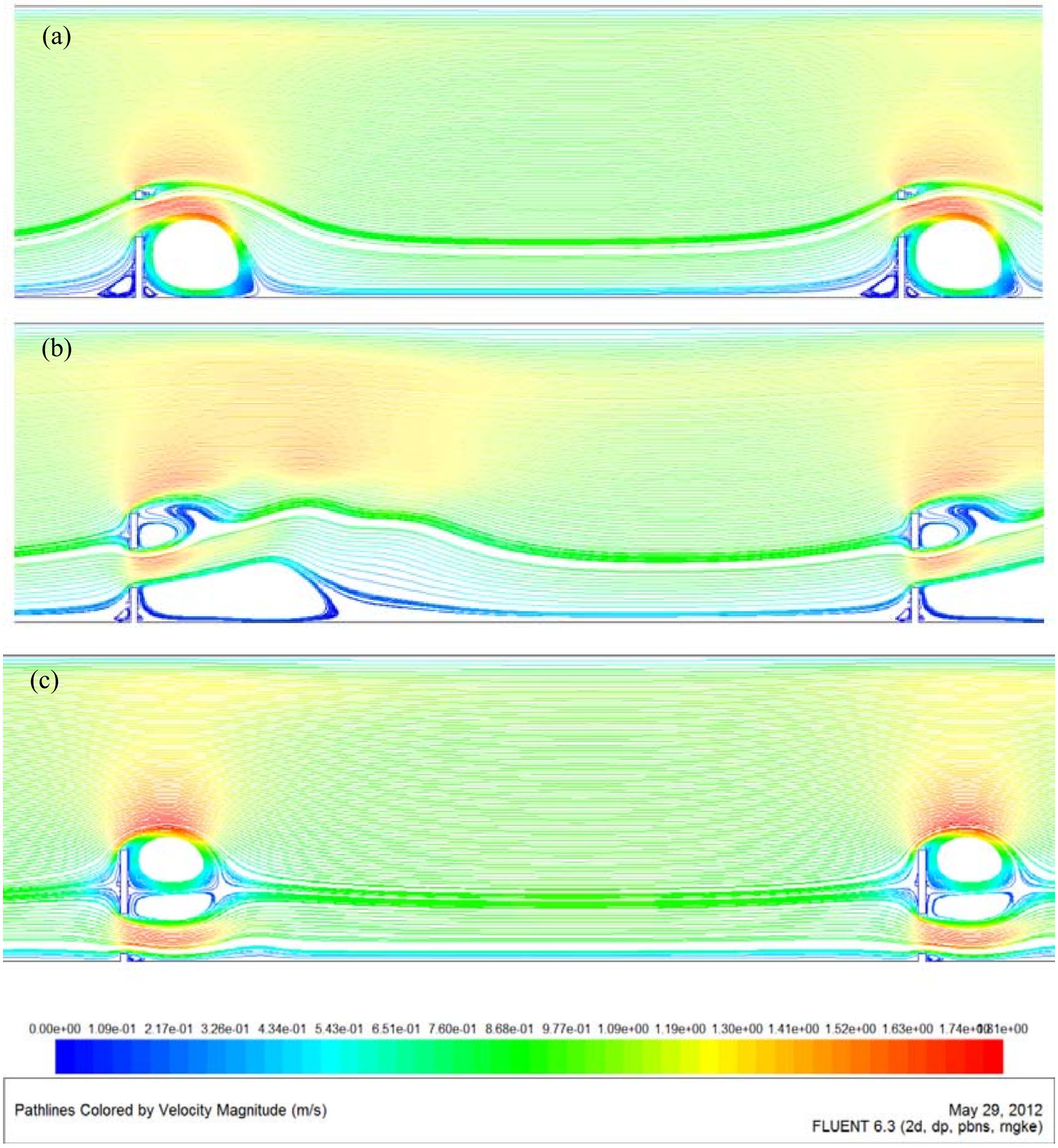

Figure 7 Path lines of e/H = 0.4, P/e = 7.21, β = 12 %, Re = 2600: (a) l/e = 0.571 (b) l/e = 0.5 (c) l/e = 0.429.

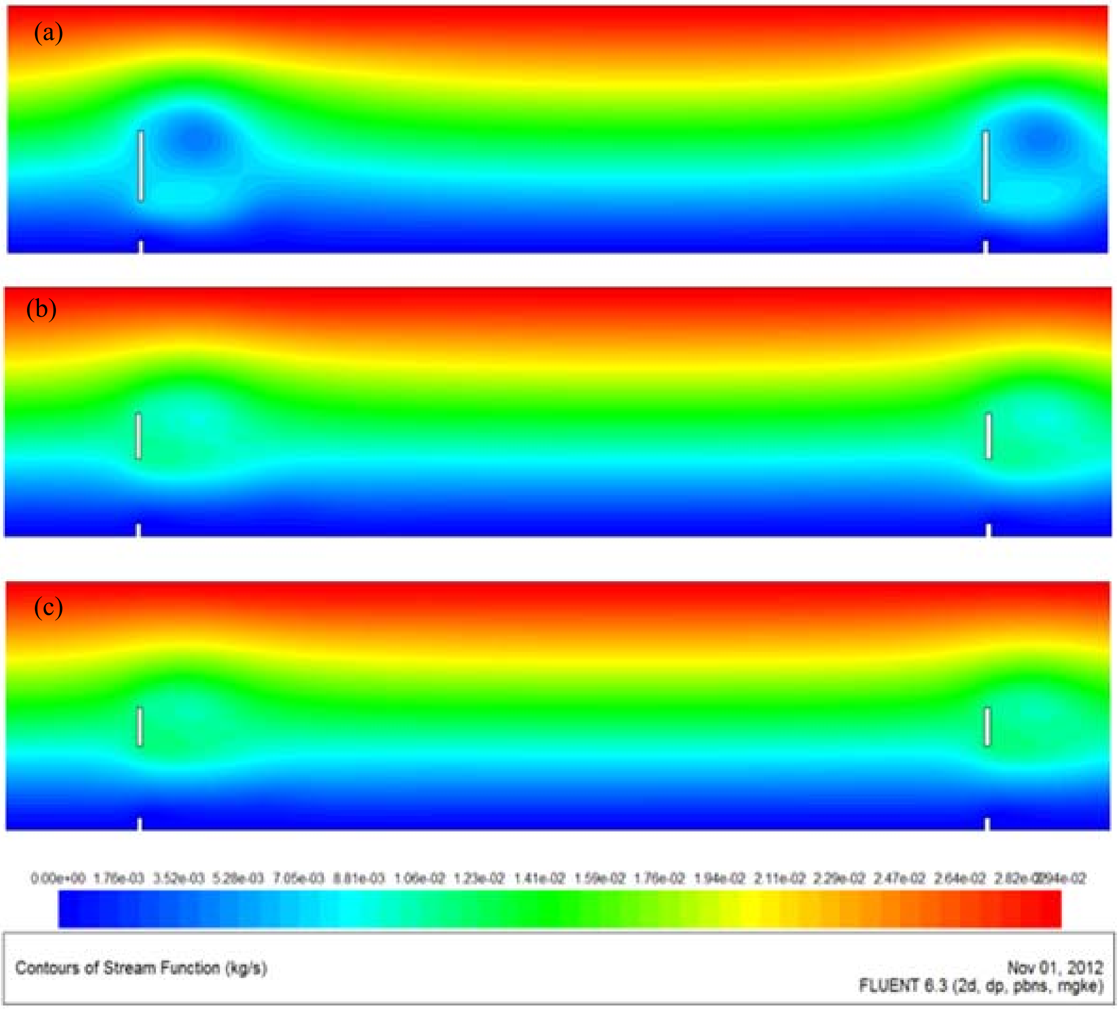

Figure 8 Contour plot of stream function of e/H = 0.4, P/e = 7.21, l/e = 0.429, Re = 2600: (a) β = 12 % (b) β = 26 % (c) β = 44 %.

Heat transfer

Figure 9 shows the Nusselt variation with the Reynolds number for 3 hole positions, and it is observed that for the range of the Reynolds number, the Nusselt number is higher for l/e = 0.429 (near to wall surface), this is due to a strong shear flow just downstream from the perforated baffles, provided by a jet like flow delivered from each hole. The perforated baffles with l/e = 0.429 possess wall jet-like flows near the heat transfer surface, resulting in a higher heat transfer. The perforated baffles with l/e = 0.5 and l/e = 0.571 influences heat transfer in a similar manner, except the good heat transfer found by jet like flow becomes less significant and the position of the area is shifted further downstream. Thus, the value of l/e = 0.429 is taken for all the test plates.

Figure 10 shows the Nusselt number variation with the Reynolds number for different relative roughness pitches and for a fixed value of relative roughness height and open area ratio. It is observed that on increasing the relative roughness pitch from 7.21 to 28.84, the Nusselt number decreases; on increasing the relative roughness pitch, the mass/heat transfer rate in the wake of the baffles reduced, as the interaction of jet like flow through holes with the reattaching and accelerating flow over the baffles is significantly reduced, causing a low heat transfer rate. In order to show the effect of relative roughness pitch more clearly, **Figure 10** is replotted in **Figure 11**, and it was observed that on increasing the relative roughness pitch, the Nusselt number decreases for all flow Reynolds number. **Figure 12** shows the effect of open area ratio on the Nusselt number; it is observed from **Figure 12** that, on increasing the open area ratio from 12 to 44 %, the Nusselt number decreases with an increase in the Reynolds number. This is due to the increase in the quantity of flow flowing through holes on increasing open area ratio; due to this, recirculation of fluid flow does not take place, as the jet spreads immediately just downstream and the interference between the jets due to the increase in the open area ratio causes less turbulence and thus results in a lesser heat transfer rate. **Figure 12** is replotted in **Figure 13** to show the effect of open area ratio and it was observed that on increasing open area ratio, the Nusselt number started decreasing.

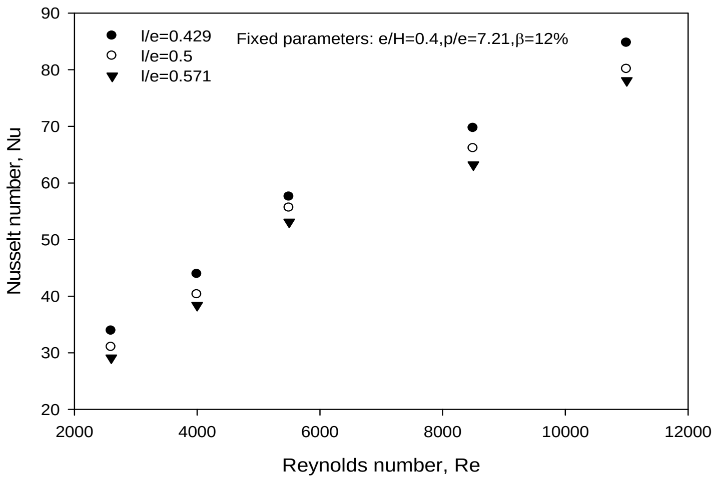

Figure 9 Effect of relative hole positions on Nusselt number.

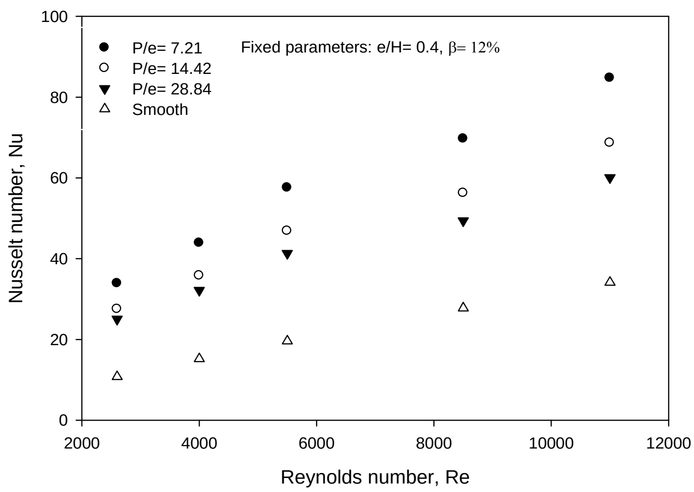

Figure 10 Variation of Nusselt number as a function of Reynolds number for different relative roughness pitch (P/e).

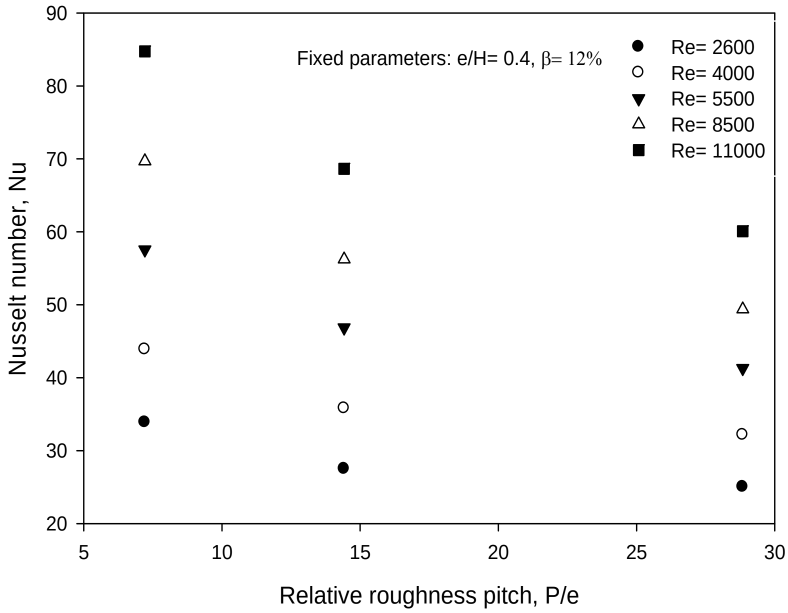

Figure 11 Variation of Nusselt number with relative roughness pitch (P/e) at different Reynolds number.

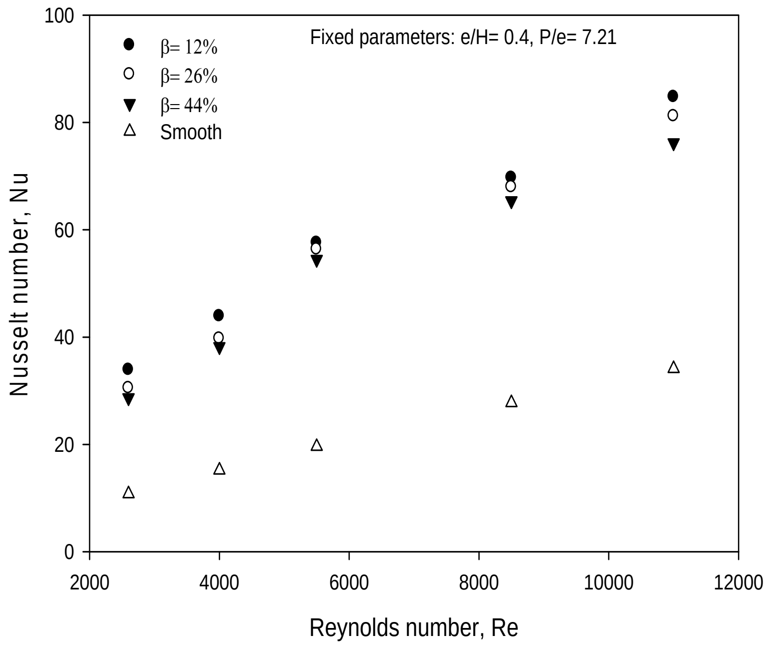

Figure 12 Variation of Nusselt number as a function of Reynolds number for different open area ratio (β).

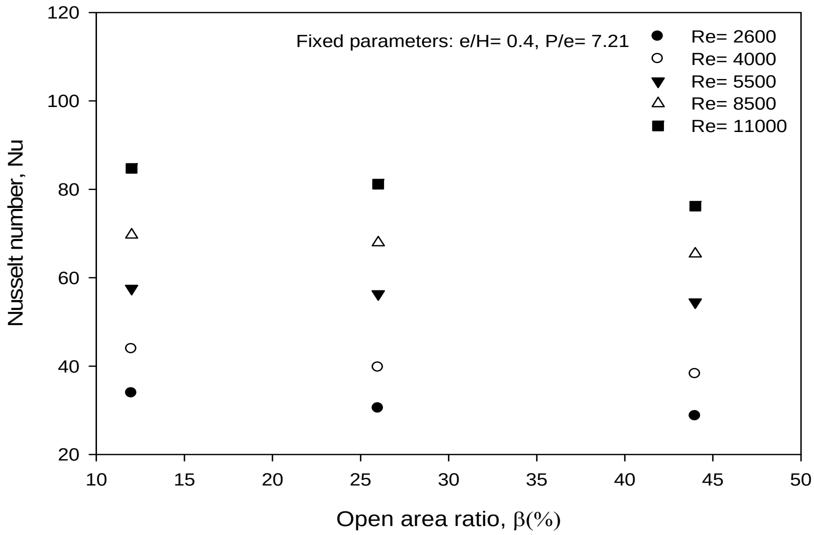

Figure 13 Variation of Nusselt number with open area ratio (β) at different Reynolds number.

Friction factor

The effect of relative roughness pitch on friction factor is shown in **Figure 14**. It is observed that, with an increase in the Reynolds number, there is a substantial increase in the friction factor over smooth duct. This can be attributed to flow blockage, higher surface area and the act caused by reverse flow. The losses mainly come from the dissipation of the dynamical pressure of air due to high viscous losses near the wall, to the extra forces exerted by the reverse flow and to higher friction of increasing surface area due to the presence of perforated baffles. **Figure 15** shows the effect of open area ratio on friction factor and it is observed that there is a considerable decrease in friction factor when increasing open area ratio from 12 to 26 %.

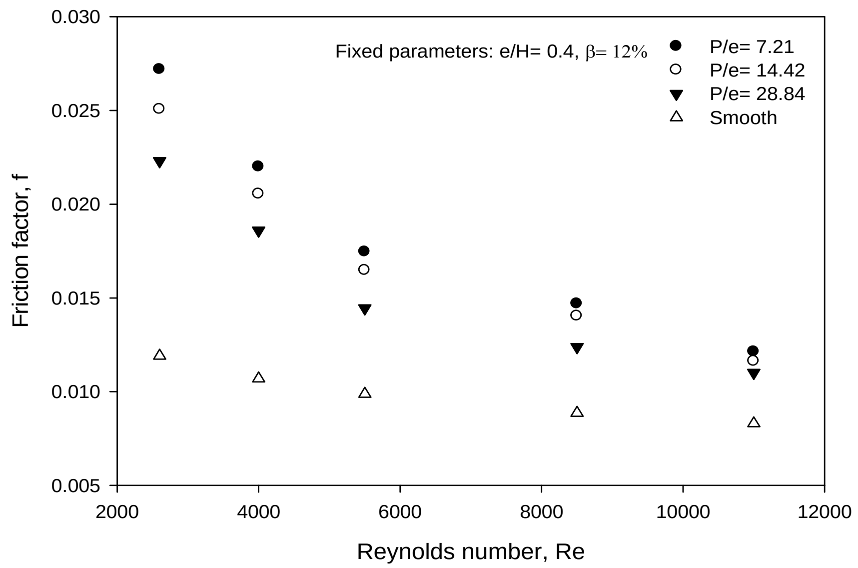

Figure 14 Effect of relative roughness pitch on friction factor.

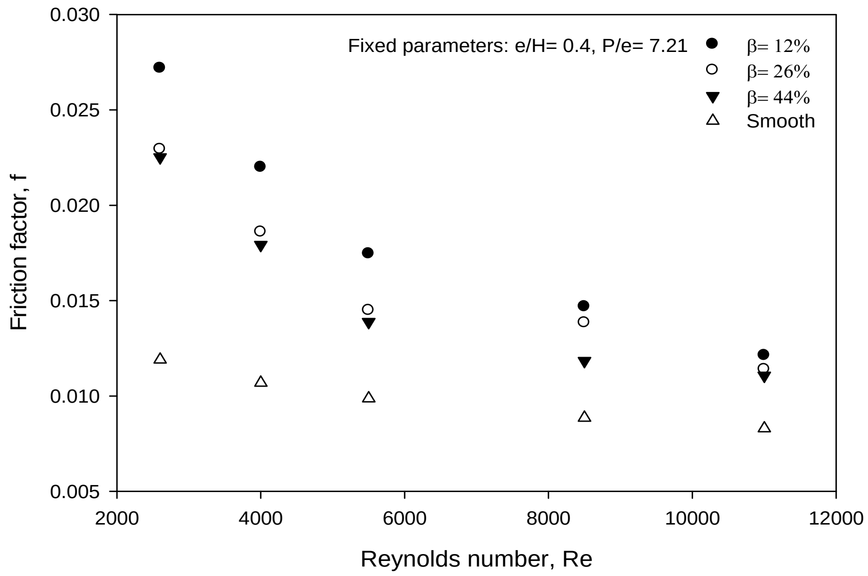

Figure 15 Effect of open area ratio on friction factor.

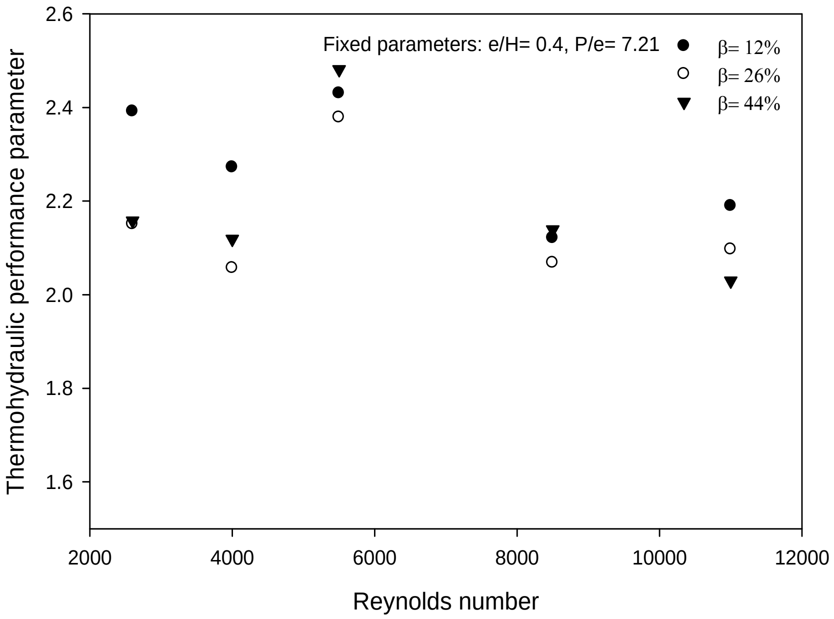

Figure 16 Thermohydraulic performance parameter as a function of Reynolds number.

Thermohydraulic performance

The thermohydraulic performance of a perforated baffled roughened solar air heater is shown in **Figure 16** and it is observed that, for the complete range of Reynolds numbers of the present study, the thermohydraulic performance parameter values are greater than unity, and the open area ratio of 12 % shows the best thermohydraulic performance for almost all Reynolds numbers. This thus signifies that the use of perforated baffled roughened solar air heaters is beneficial for designers and can be used in space heating and in agriculture for crop drying.

Development of Nusselt number and friction factor correlations

It is revealed from numerical data that the Nusselt number and friction factor are strong functions of flow and geometrical parameter. The functional relationship for the Nusselt number and friction factor can be written as;

$$Nu = f_1\left(\mathrm{Re}, \frac{P}{e}, \beta\right) \tag{10}$$

$$f = f_2\left(\mathrm{Re}, \frac{P}{e}, \beta\right) \tag{11}$$

In order to obtain the performance of roughened duct having transverse perforated baffles as roughness elements, the Nusselt number and friction factor correlation were developed for flow and geometrical parameters by the following procedure, reported by [9]. Sigma plot software has been used to carry out regression analysis.

Nusselt number correlation

Numerical data of the Nusselt number was plotted on a log-log scale as shown in **Figure 17**. It shows that the Nusselt number and the Reynolds number have almost a linear relationship. From regression analysis it has been found that the average slope of all the lines is 0.6244. The straight line equation is represented as;

$$Nu = A_O \mathrm{Re}^{0.6244} \tag{12}$$

The coefficient A_o is a function of other influencing parameters. Taking relative roughness pitch (P/e) into consideration and plotting between $\ln\left[\frac{NU}{\mathrm{Re}^{0.6244}}\right]$ and $\ln\left[\frac{P}{e}\right]$, as shown in **Figure 18,** a regression analysis to fit straight lines through these points is given by;

$$Nu = B_O \mathrm{Re}^{0.6244}\left(\frac{P}{e}\right)^{-0.3189} \tag{13}$$

The coefficient B_o is a function of other influencing parameters. Taking open area ratio (β) into consideration and plotting between;

$\ln\left[\frac{NU}{\mathrm{Re}^{0.6244}\left(\frac{P}{e}\right)^{-0.3189}}\right]$ and $\ln(\beta)$ as shown in **Figure 19,** a regression analysis to fit a second order polynomial is given by;

$$Nu = C_O \mathrm{Re}^{0.6244}\left(\frac{P}{e}\right)^{-0.3189}(\beta)^{0.4428} \exp\left(-0.0822\ln(\beta)^2\right) \tag{14}$$

The value of coefficient C_o is 0.28 and the final correlation for the Nusselt number is written as;

$$Nu = 0.28\,\mathrm{Re}^{0.6244}\left(\frac{P}{e}\right)^{-0.3189}(\beta)^{0.4428} \exp\left(-0.0822\ln(\beta)^2\right) \tag{15}$$

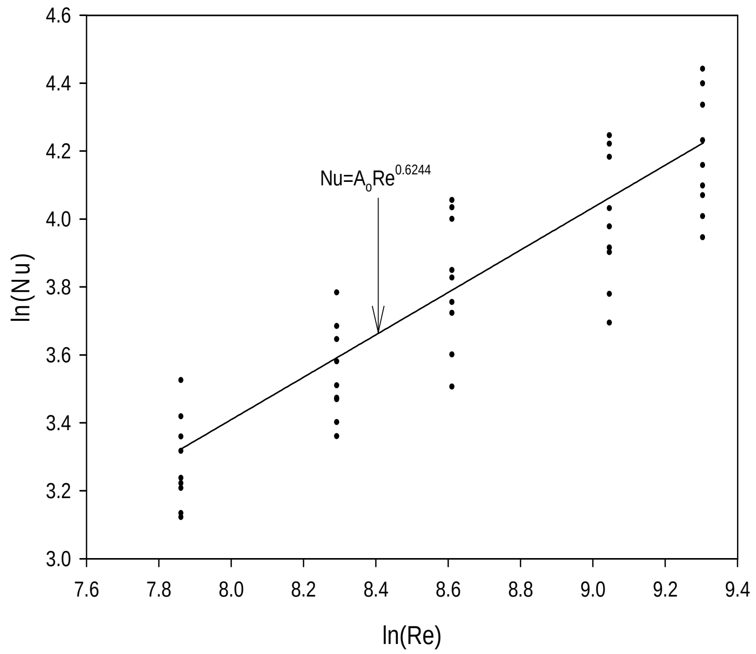

Figure 17 Plot of ln(Nu) as function of ln(Re) for all numerical data.

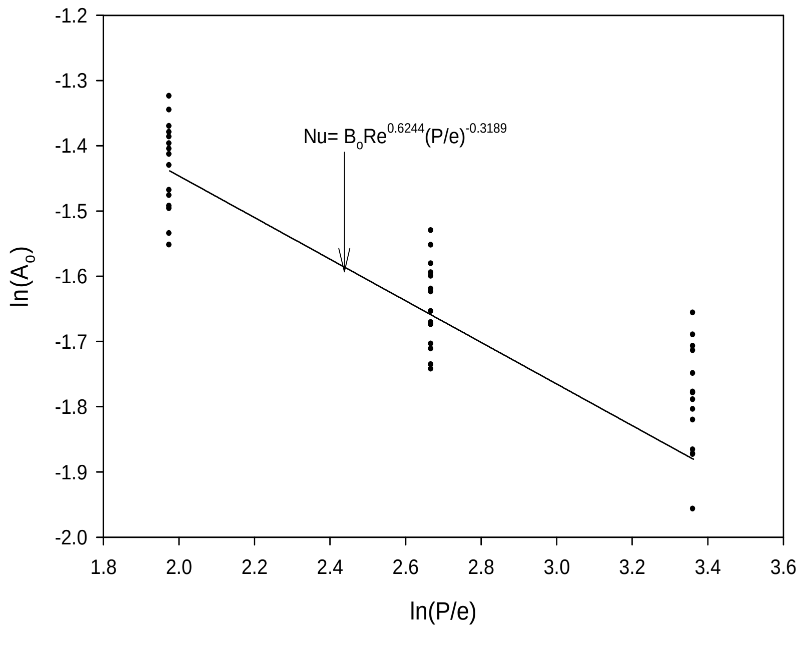

Figure 18 Plot of $\ln(A_o)$ as function of ln(P/e).

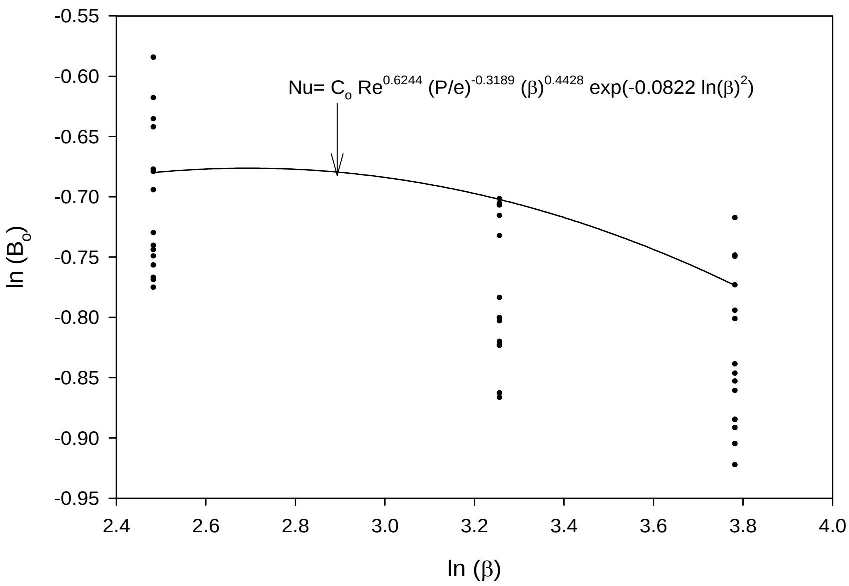

Figure 19 Plot of $\ln(B_o)$ as function of $\ln(\beta)$.

Correlation for friction factor

A similar procedure has been employed to develop correlation for the friction factor as shown in **Figures 20 - 22**, and is obtained as follows.

$$f = 1.975\,\mathrm{Re}^{-0.4989}\left(\frac{P}{e}\right)^{-0.0386}(\beta)^{-0.2032}\exp\left(0.0212\ln(\beta)^2\right) \tag{16}$$

The equation is the final correlation for the friction factor.

Validity of the Nusselt number and friction factor correlation can be seen by their values using Eqs. (15) and (16). The values of correlations of the Nusselt number and friction factor lie within ± 15 and ± 13 % respectively of numerically determined values. An average absolute deviation of 3.28 and 4.06 % in the Nusselt number and friction factor between predicted and numerical values was observed, showing a good agreement between predicted and numerical results, and is shown in **Figures 23** and **24**. Hence, for the range of parameters investigated, the Nusselt number and friction factor can be predicted with reasonable precision using correlations in Eqs. (15) and (16).

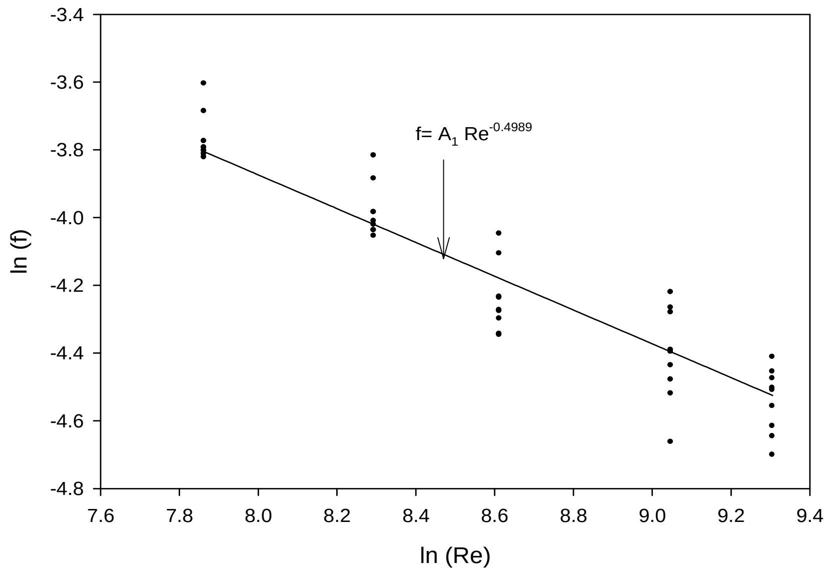

Figure 20 Plot of ln(f) as function of ln(Re) for all numerical data.

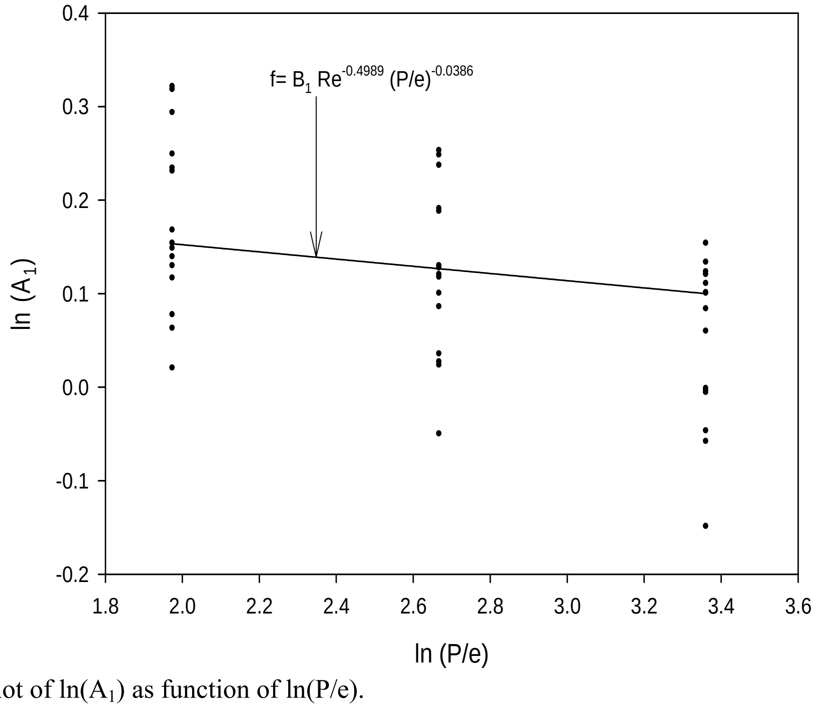

Figure 21 Plot of $\ln(A_1)$ as function of ln(P/e).

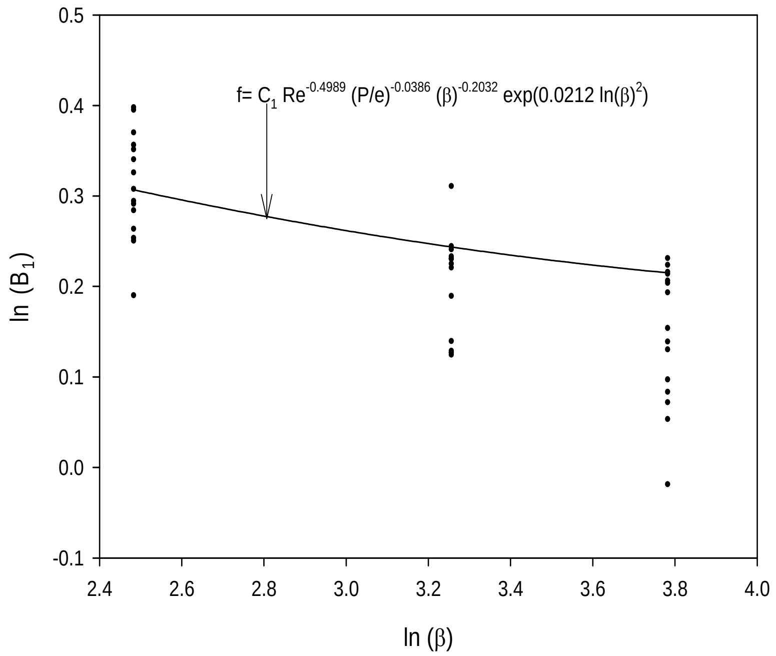

Figure 22 Plot of $\ln(B_1)$ as function of $\ln(\beta)$.

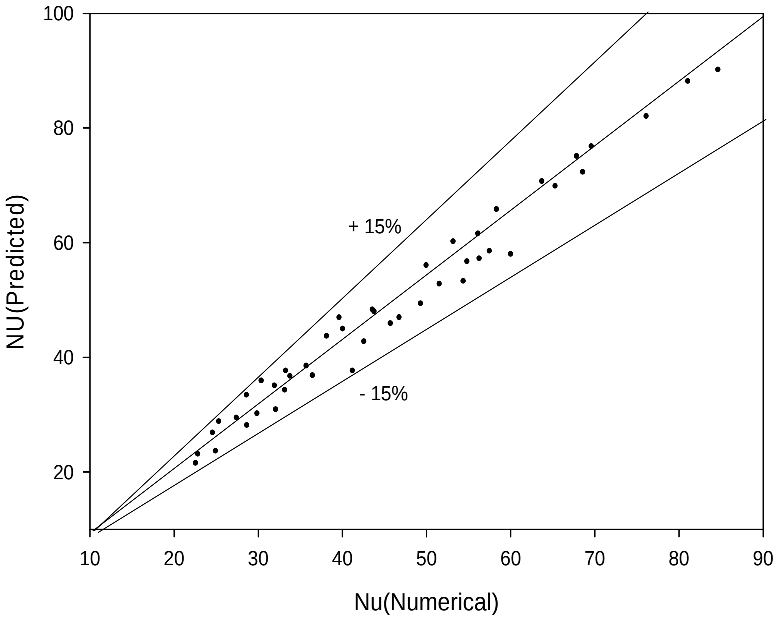

Figure 23 Comparison of numerical and predicted values of Nusselt number.

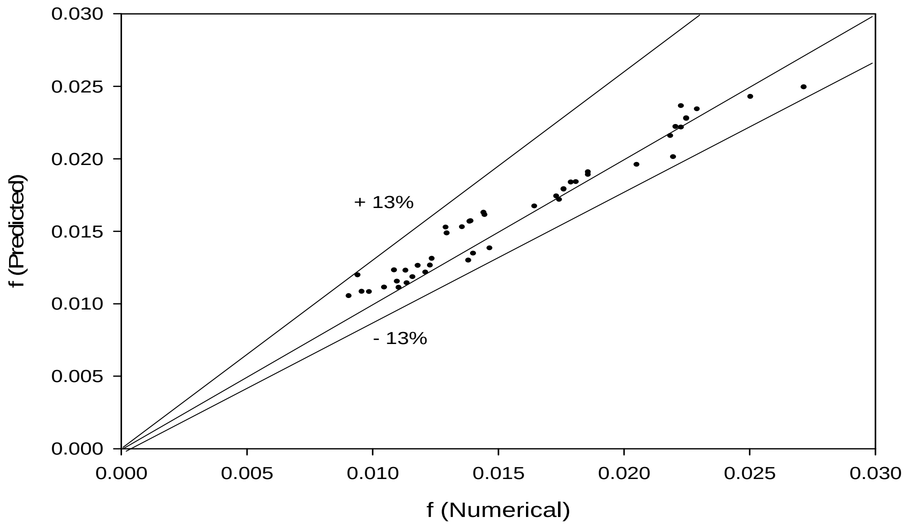

Figure 24 Comparison of numerical and predicted values of friction factor.

Conclusions

Based on the numerical investigations of heat and fluid flow in a rectangular duct with transverse perforated baffles as roughness elements on 1 broad wall subjected to a uniform heat flux, the following conclusions were drawn.

1. Verification of the heat transfer results is performed by comparing with the previous experimental results. The RNG k-ε turbulence model is found to be suitable for the prediction of heat transfer and flow friction in perforated baffled roughened duct.

2. The maximum enhancement and friction factor due to presence of perforated baffles as roughness element has been found to be times 3.1 and 2.2, respectively in comparison to the smooth duct for the range of geometrical and flow parameters considered.

3. The maximum heat transfer enhancement and maximum friction factor value attained for relative roughness pitch (P/e) has a value of 7.21 and open area ratio (β) has a value of 12 %.

4. Statistical correlations have been developed for the Nusselt number and friction factor as function of geometrical and flow parameters. For these correlations the average absolute deviation of the Nusselt number and friction factor are 3.28 and 4.06 %, respectively.

References

[1] Z Hu and J Shen. Heat transfer enhancement in a converging passage with discrete ribs. *Int. J. Heat Mass Tran.* 1996; **39**, 1719-27.

[2] AME Momin, JS Saini and SC Solanki. Heat transfer and friction in solar air heater duct with V-shaped rib roughness on absorber plate. *Int. J. Heat Mass Tran.* 2002; **45**, 3383-96.

[3] R Karwa. Experimental studies of augmented heat transfer and friction in asymmetrically heated rectangular ducts with ribs on the heated wall in transverse, inclined, v-continuous and v-discrete pattern. *Int. Comm. Heat Mass Tran.* 2003; **30**, 241-50.

[4] SV Karmare and AN Tikekar. Heat transfer and friction factor correlation for artificially roughened duct with metal grit ribs. *Int. J. Heat Mass Tran.* 2007; **50**, 4342-51.

[5] KR Aharwal, BK Gandhi and JS Saini. Experimental investigation on heat-transfer enhancement due to a gap in an inclined continuous rib arrangement in a rectangular duct of solar air heater. *Renew. Energ.* 2008; **33**, 585-96.

[6] Varun, RP Saini and SK Singal. Investigation of thermal performance of solar air heater having roughness elements as a combination of inclined and transverse ribs on the absorber plate. *Renew. Energ.* 2008; **33**, 1398-405.
[7] SK Saini and RP Saini. Development of correlations for Nusselt number and friction factor for solar air heater with roughened duct having arc-shaped wire as artificial roughness. *Sol. Energ.* 2008; **82**, 1118-30.
[8] VS Hans, RP Saini and JS Saini. Heat transfer and friction factor correlations for a solar air heater duct roughened artificially with multiple v ribs. *Sol. Energ.* 2010; **84**, 898-1.
[9] S Singh, S Chander and JS Saini. Heat transfer and friction factor correlations of solar air heater ducts artificially roughened with discrete v-down ribs. *Energy* 2011; **36**, 5053-64.
[10] R Karwa, SC Solanki and JS Saini. Heat transfer coefficient and friction factor correlations for the transitional flow regime in rib-roughened rectangular ducts. *Int. J. Heat .Mass Tran.* 1999; **42**, 1597-615.
[11] RP Saini and JS Saini. Heat transfer and friction factor correlations for artificially roughened ducts with expended metal mesh as roughness element. *Int. J. Heat Mass Tran.* 1997; **40**, 973-86.
[12] S Sripattanapipat and P Promvonge. Numerical analysis of laminar heat transfer in a channel with diamond shaped baffles. *Int. Comm. Heat Mass Tran.* 2009; **36**, 32-8.
[13] SB Bopche and MS Tandale. Experimental investigation on heat transfer and frictional characteristics of a turbulator roughened solar air heater duct. *Int. J. Heat Mass Tran.* 2009; **52**, 2834-48.
[14] P Promvonge. Heat transfer and pressure drop in a channel with multiple 60^o V Baffles. *Int. Comm. Heat Mass Tran.* 2010; **37**, 835-40.
[15] P Promvonge, W Jedsadaratanachai and S Kwankaomeng. Numerical study of laminar flow and heat transfer in square channel with 30^o inline angled baffle turbulators. *Appl. Therm. Eng.* 2010; **30**, 1292-303.
[16] S Kwankaomeng and P Promvonge. Numerical prediction on laminar heat transfer in square duct with 30^o angled baffle on one wall. *Int. Comm. Heat Mass Tran.* 2010; **37**, 857-66.
[17] P Promvonge and S Kwankaomeng. Periodic laminar flow and heat transfer in a channel with 45^o staggered V baffles. *Int. Comm. Heat Mass Tran.* 2010; **37**, 841-9.
[18] M Molki and AR Mostoufizadeh. Turbulent heat transfer in rectangular ducts with repeated baffle blockages. *Int. J. Heat Mass Tran.* 1989; **32**, 1491-9.
[19] JJ Hwang and TM Liou. Heat transfer in a rectangular channel with perforated turbulence promoters using holographic interferometry measurement. *Int. J. Heat Mass Tran.* 1995; **38**, 3197-207.
[20] JJ Hwang, TY Lia and TM Liou. Effect of fence thickness on pressure drop and heat transfer in a perforated fenced channel. *Int. J. Heat Mass Tran.* 1998; **41**, 811-6.
[21] TM Liou and SH Chen. Turbulent heat and fluid flow in a passage distributed by detached perforated ribs of different heights. *Int. J. Heat Mass Tran.* 1998; **41**, 1795-806.
[22] Dutta and Dutta. Effect of baffle size, perforation, and orientation on internal heat transfer enhancement. *Int. J. Heat Mass Tran.* 1998; **41**, 3005-13.
[23] P Dutta, A Hossain. Internal cooling augmentation in rectangular channel using two inclined baffles. *Int. J. Heat Fluid Flow* 2005; **26**, 223-32.
[24] R Karwa, BK Maheshwari and N Karwa. Experimental study of heat transfer enhancement in an asymmetrically heated rectangular duct with perforated baffles. *Int. Comm. Heat Mass Tran.* 2005; **32**, 275-84.
[25] KD Huang, SC Tzeng, TM Jeng and JR Wang, SY Cheng and KT Tseng. Experimental study of fluid flow and heat transfer characteristics in the square channel with a perforation baffle. *Int. Comm. Heat Mass Tran.* 2008; **35**, 1106-12.
[26] R Karwa and BK Maheshwari. Heat transfer and friction in an asymmetrically heated rectangular duct with half and fully perforated baffles at different pitches. *Int. Comm. Heat Mass Tran.* 2009; **36**, 264-8.
[27] SV Patankar. *Numerical Heat Transfer and Fluid Flow*. McGraw Hill, New York, 1980.